Entanglement formation between magnon and center-of-mass motion of a levitated particle in a magnomechanical system

S. Bayati [1,*] A. Mahdifar,[1,2,†] and M. Bagheri Harouni [1,2,‡]
[1]*Department of Physics, University of Isfahan, Hezar Jerib, 81746-73441 Isfahan, Iran*
[2]*Quantum Optics Group, Department of Physics, University of Isfahan, Hezar Jerib, 81746-73441 Isfahan, Iran*

(Received 25 January 2024; accepted 24 June 2024; published 22 July 2024)

Entanglement formation between the magnons as the internal degrees of freedom and the center-of-mass motion (CM) as the external degrees of freedom of a levitated yttrium iron garnet (YIG) sphere in a cavity-magnomechanical system is studied. Here, we propose a scheme for generating magnon-CM entanglement independent from the mass and size of the sphere in the hybrid magnonic system by driving the magnon with the parametric amplification. First, we show that the power and frequency of the driving field significantly affect this entanglement, since the driving field increases effective magnon-CM coupling. But, by increasing the magnon damping rate, this entanglement considerably decreases. Moreover, in the next step, we demonstrate the manipulation and enhancement of this entanglement by driving the magnon into the squeezed state. Our results present an approach for preparing quantum states and may find promising applications in the quantum metrology and sensing.

DOI: 10.1103/PhysRevA.110.013710

I. INTRODUCTION

Magnetic materials have emerged as a compelling alternative for achieving robust light-matter interactions. The advent of hybrid magnonic systems has introduced a new type of quantum system that is based on magnons (collective spin excitations) of a ferromagnetic crystal such as yttrium iron garnet (YIG) which provides unique properties, i.e., high spin density and low damping rate, as well as offers a promising avenue for exploring the frontiers of quantum technologies. Magnons have been extensively investigated because of their long coherence times [1–5] as well as their potential for coupling with other quantum excitations, such as other magnons [6], spin qubits [7,8], and optical and microwave photons [9–12]. Furthermore, magnons could couple to deformation phonons through magnetostrictive force [13,14] and the center-of-mass motion (CM) through an inhomogeneous driving field [7,8,15], which may open up a new way to thoroughly study quantum phenomena and promising applications in quantum communication and information. In other words, various magnonic-based hybrid quantum systems have led to some interesting effects, e.g., ground-state cooling of the mechanical vibration mode [16,17], spin current control [18,19], magnon-phonon entanglement, magnon-squeezed states [20–26], coherent optical-to-microwave conversion [27,28], and magnon-induced nonreciprocity [29,30]. Additionally, intriguing applications have been investigated in such hybrid systems, such as precision measurements [31–34], long-time memory [35,36], ultraslow light engineering [37,38], magnon lasers [39,40], quantum thermometry [41], and magnon-photon manipulation using exceptional points [42–46].

On the other hand, it is noteworthy that a magnet particle can be trapped using various techniques, for example, with an ion trap [47], with a magnetic trap [48,49], with an optical trap [50], or by being clamped to an ultrahigh-Q mechanical resonator [51]. In addition, alternative levitation methods, such as magnetic levitation in a microwave cavity [52] or floating above a superconductor in free space [53,54], have the potential to levitate and cool millimeter-sized spherical magnets. So, besides the magnonic system, levitated objects offer a robust platform for exploring the boundary between the classical and quantum realms with massive objects [55,56]. Moreover, their weak coupling to the environment and their capability to cool their center-of-mass motion make them ideal systems for sensing weak forces [57,58]. Intriguing possibilities have been proposed for interacting systems comprising levitated particles, consisting of dark matter detection [59] and measurement of quantum gravity [60]. Beyond these significant aspects, levitated systems provide an excellent framework for studying nonequilibrium physics [61]. Furthermore, using these quantum systems for ultrasensitive force detection opens up innovative avenues for commercial sensing applications [62].

Quantum entanglement stands out as a remarkable aspect of quantum mechanics. This quantum effect plays an important role in different applications, including quantum metrology [63], quantum computing [64], quantum memory [65], and quantum teleportation [66,67]. Quantum entanglement not only facilitates the development of quantum technologies but also contributes to a deeper understanding of the quantum behaviors exhibited by quantum systems. Moreover, entangled states naturally have a key role in quantum

*Contact author: phsnbayati@gmail.com
†Contact author: ali.mahdifar@sci.ui.ac.ir
‡Contact author: m-bagheri@phys.ui.ac.ir

control experiments when studying the nonclassical phenomena [68]. In addition, squeezed states, crucial quantum states, play a significant role in quantum measurement. For instance, squeezed light can enhance the sensitivity of interferometers in gravitational-wave detection [69,70], generate an entangled source for quantum teleportation [71], and improve the entangled state [72,73]. So, due to these exceptional characteristics of squeezed states, various approaches have been suggested to prepare squeezed states of magnons and photons based on magnonic systems, e.g., applying ferromagnetic anisotropy [74], employing a two-tone microwave field to drive the magnon mode [75], and transferring squeezing from a squeezed vacuum microwave [26].

As we know, the ability to generate the entanglement is at the center of most protocols in quantum information and quantum processing. Also, motivated by the features of magnonic and levitated systems, we are interested in studying the entanglement between magnons as the internal degrees of freedom and the CM as the external degrees of freedom associated with a levitated particle in a hybrid magnonic system.

To this end, in the present paper, we consider a microwave cavity magnomechanical system, composed of a levitated YIG sphere. Additionally, in the proposed magnomechanical system we propose a parametric amplification drive for the magnon subsystem to prepare the magnon squeezed state. We demonstrate that we can enhance and manipulate the entanglement by magnon squeezing.

The obtained magnon-CM entanglement (MCE) has the following properties. It is independent of the size and mass of the YIG sphere and is increased by increasing the driving field. Although the MCE is sensitive to the temperature, we can preserve it up to higher temperatures by assuming magnon squeezing. In other words, magnon squeezing plays a compensation role against the temperature increasing. Also, the MCE between the external and internal degrees of freedom has potential applications in the study of macroscopic quantum phenomena. Moreover, utilizing these external degrees of freedom enables manipulation of the magnon degrees of freedom.

The paper is organized as follows. In Sec. II the quantum system is introduced, and then the dynamics of the system is investigated through the quantum Langevin-Heisenberg equations of motion. The numerical results are studied in Sec. III. Finally, the conclusion and outlook are given in Sec. IV.

II. THE SYSTEM AND HAMILTONIAN

The system we are going to investigate is a cavity-magnomechanical system with a levitated YIG sphere whose center of mass is trapped in a harmonic oscillator potential. In addition, a homogeneous magnetic field is applied on the sphere to excite the magnon modes [76,77]. A schematic of the system under study is shown in Fig. 1. The Hamiltonian of the system can be decomposed to the following three contributions:

$$\hat{H} = \hat{H}_0 + \hat{H}_{\rm int} + \hat{H}_d. \tag{1}$$

The first term $\hat{H}_0$ is the free Hamiltonian, given by

$$\hat{H}_0/\hbar = \omega_a \hat{a}^\dagger \hat{a} + \omega_m \hat{m}^\dagger \hat{m} + \frac{\omega_c}{2}\left(\hat{x}^2 + \hat{p}_x^2\right), \tag{2}$$

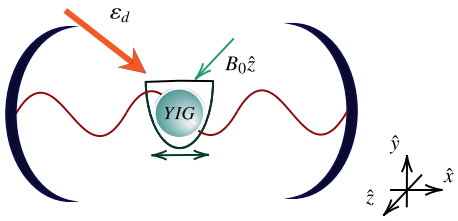

FIG. 1. Schematic of the cavity which consists of the levitated YIG sphere and is driven by an external field.

where the first two terms describe the cavity and the magnonic modes, with the bosonic annihilation operators $\hat{a}$ and $\hat{m}$ with frequencies ω_a and ω_m, respectively. In the third term, $\hat{x}$ and $\hat{p}_x$ are the position and momentum operators of the magnetic particle CM that oscillates at ω_c, the frequency of the trap.

The second term, $\hat{H}_{\rm int}$, in the Hamiltonian (1) describes the interaction between the magnon and photon modes as

$$\hat{H}_{\rm int}/\hbar = g_{am}(\hat{a}^\dagger \hat{m} + \hat{a}\hat{m}^\dagger)\cos(k\,x), \tag{3}$$

where we have used the rotating-wave approximation. As is known, the magnon-photon coupling which is characterized by the magnetic dipole interaction, $H_{\rm int} = -\vec{m}\cdot\vec{B}_{\rm cav}$, can be studied as the coupling between a microwave cavity mode and the Kittel magnon [8,9,15]. It is worth mentioning that the magnon frequency is determined by the external magnetic field B_0 and the gyromagnetic ratio $\gamma/2\pi = 28$ GHz/T as $\omega_m = \gamma B_0$. Moreover, we assumed that the cavity mode along $\hat{y}$ direction has the form as $\vec{B}_{\rm cav} = \hat{y}B\cos(kx)$, where k is the microwave field wave number [15]. The magnon-photon coupling strength is $g_{am} = \frac{\gamma}{2}\sqrt{\frac{\hbar\omega_a\mu_0}{V_a}}\sqrt{2\rho_s V s}$, in which V_a and V are the mode volume of the cavity mode and the volume of the YIG sphere, respectively, $s = \frac{5}{2}$ is the spin number of the YIG's ground state, μ_0 is the vacuum permeability, and ρ_s is the spin density of the YIG sphere. Here, we focus on the Kittle magnon mode which is the homogeneous ground state of the magnonic mode and can be simply tuned by B_0.

The last term, $\hat{H}_d$, in Hamiltonian (1) represents the driving of the cavity mode and the magnon mode with parametric amplification:

$$\hat{H}_d/\hbar = \varepsilon_d(\hat{a}^\dagger e^{-i\omega_d t} - \hat{a}e^{i\omega_d t}) + \frac{i\rho}{2}(\hat{m}^{\dagger 2}e^{i\theta}e^{-i\omega_0 t} + \hat{m}^2 e^{-i\theta}e^{i\omega_0 t}), \tag{4}$$

where ω_d is frequency of an external laser which drives the cavity mode with the amplitude $\varepsilon_d = \sqrt{\frac{2\gamma_a P_d}{\hbar\omega_d}}$. Here, γ_a and P_d denote the cavity decay rate and the power of the input drive field, respectively. Moreover, the last term in H_d represents the squeezing of the magnonic mode where ρ and θ are the squeezing parameter and phase. It should be noted that magnon squeezing can be realized by, e.g., squeezing from the cavity with a squeezed vacuum field [26], using the anisotropy of the ferromagnet [74], or driving a qubit with two microwave fields in cavity-magnon-qubit systems [75].

By expanding $\cos(kx)$ up to the first order in x around the minimum position of the trap, x_0, and supposing $\omega_d = \omega_0$, the total Hamiltonian (1) in the frame rotating at this frequency is given by

$$\begin{aligned}\hat{H}/\hbar = {} & \Delta_a \hat{a}^\dagger \hat{a} + \Delta_m \hat{m}^\dagger \hat{m} + \omega_c \hat{c}^\dagger \hat{c} \\ & + (\hat{a}\hat{m}^\dagger + \hat{a}^\dagger \hat{m})[g_{am}\cos(kx_0) - g_{\rm amc}\sin(kx_0)(\hat{c}^\dagger + \hat{c})] \\ & + \varepsilon_d(\hat{a}^\dagger - \hat{a}) + \frac{i\rho}{2}(\hat{m}^{\dagger 2} e^{i\theta} + \hat{m}^2 e^{-i\theta}),\end{aligned} \tag{5}$$

where $\Delta_j = \omega_j - \omega_d$ ($j = a$ and m) is the detuning between the photon and magnon excitations concerning the driving field and $\hat{c}$ is the annihilation operator of the CM oscillation. Also, the photon-magnon-CM coupling strength is determined by $g_{\rm amc} = g_{am} k \sqrt{\frac{\hbar}{2\rho_m V \omega_s}}$, where the YIG sphere's mass density is $\rho_m = 5170\,{\rm kg\ m^{-3}}$. It should be noted that $g_{\rm amc}$ is independent of the sphere's mass and size and the Kittel magnon frequency can be adjusted to rather close to on-resonance with the cavity mode.

Dynamics of the system

By employing the quantum Langevin equations (QLEs), which are obtained by adding damping and noise terms to the Heisenberg equations [78], we can describe the dynamics of cavity, magnonic, and levitated particle CM subsystems as follows:

$$\begin{aligned}\dot{\hat{a}} = {} & -\left(\frac{\gamma_a}{2} + i\Delta_a\right)\hat{a} + i\, g_{\rm amc}\, \sin(kx_0)\, \hat{m}\, (\hat{c} + \hat{c}^\dagger) - i\varepsilon_d \\ & - i\, g_{am}\cos(kx_0)\, \hat{m} + \sqrt{\gamma_a}\hat{a}^{\rm in}, \\ \dot{\hat{m}} = {} & -\left(\frac{\gamma_m}{2} + i\Delta_m\right)\hat{m} + i\, g_{\rm amc}\, \sin(kx_0)\, \hat{a}\, (\hat{c} + \hat{c}^\dagger) + \rho e^{i\theta}\hat{m}^\dagger \\ & - i\, g_{am}\cos(kx_0)\, \hat{a} + \sqrt{\gamma_m}\hat{m}^{\rm in}, \\ \dot{\hat{c}} = {} & -\left(\frac{\gamma_c}{2} + i\omega_c\right)\hat{c} + i\, g_{\rm amc}\sin(kx_0)\, (\hat{a}\hat{m}^\dagger + \hat{a}^\dagger \hat{m}) + \sqrt{\gamma_c}\hat{c}^{\rm in}.\end{aligned} \tag{6}$$

Here, γ_o ($o = a$, m, and c) is the related damping rate, and the noise operator $\hat{o}^{\rm in}$ is considered to satisfy the following correlation functions:

$$\begin{aligned}\langle \hat{o}^{\rm in}(t)\hat{o}^{\rm in\dagger}(t')\rangle &= (\bar{n}_o + 1)\delta(t - t'), \\ \langle \hat{o}^{\rm in\dagger}(t)\hat{o}^{\rm in}(t')\rangle &= \bar{n}_o \delta(t - t'),\end{aligned} \tag{7}$$

where $\bar{n}_o = [e^{(\frac{\hbar\omega_o}{k_B T})} - 1]^{-1}$ is the bosonic mode's mean thermal occupation, T is the temperature of the thermal environment, and k_B is the Boltzmann constant. In order to find the solutions of the nonlinear QLEs in Eqs. (6), we decompose each operator as the sum of its steady-state value and a small fluctuation as $\hat{o} = o_0 + \delta\hat{o}$, and we ignore small second-order fluctuation terms. The equations of the steady-state mean values of the system are obtained as

$$\begin{aligned}\dot{a}_0 = {} & -\left(\frac{\gamma_a}{2} + i\Delta_a\right)a_0 - i(G_{am} + 2G_{\rm amc}{\rm Re}[c_0])m_0 - i \\ & \varepsilon_d = 0, \\ \dot{m}_0 = {} & -\left(\frac{\gamma_m}{2} + i\Delta_m\right)m_0 - i(G_{am} + 2G_{\rm amc}{\rm Re}[c_0]) \\ & a_0 + \rho e^{i\theta} = 0, \\ \dot{c}_0 = {} & -\left(\frac{\gamma_c}{2} + i\omega_c\right)c_0 - iG_{\rm amc}(a_0 m_0^* + a_0^* m_0) = 0,\end{aligned} \tag{8}$$

where $G_{\rm amc} = -g_{\rm amc}\sin(kx_0)$ (which has small experimental value) and $G_{am} = g_{am}\cos(kx_0)$. Furthermore, we suppose that the YIG sphere is located at the node of the cavity magnetic field, which is $k\,x_0 = (2n+1)\pi/2$ [15]. On the other hand, the levitation developments enable us to control the particle position [56]. Therefore, we could achieve $G_{am} = 0$ and $G_{\rm amc} = -g_{\rm amc}$ via controlling the particle position. Also, we assume that $|\rho| \ll |\varepsilon_d|$. With these assumptions, we can obtain stable solutions. So, the steady-state values are obtained as follows:

$$a_0 \simeq \frac{-i\varepsilon_d}{\gamma_a/2 + i\Delta_a},\ m_0 = c_0 \simeq 0. \tag{9}$$

Besides, the linearized QLEs for the quantum fluctuations are obtained as follows:

$$\begin{aligned}\delta\dot{\hat{a}}(t) = {} & -\left(\frac{\gamma_a}{2} + i\Delta_a\right)\delta\hat{a} + \sqrt{\gamma_a}\hat{a}^{\rm in}, \\ \delta\dot{\hat{m}}(t) = {} & -\left(\frac{\gamma_m}{2} + i\Delta_m\right)\delta\hat{m} - ig_{\rm eff}(\delta\hat{c} + \delta\hat{c}^\dagger) + \rho e^{i\theta}\delta\hat{m}^\dagger \\ & + \sqrt{\gamma_m}\hat{m}^{\rm in}, \\ \delta\dot{\hat{c}}(t) = {} & -\left(\frac{\gamma_c}{2} + i\omega_c\right)\delta\hat{c} - ig_{\rm eff}(\delta\hat{m}^\dagger + \delta\hat{m}) + \sqrt{\gamma_c}\hat{c}^{\rm in},\end{aligned} \tag{10}$$

where $g_{\rm eff} = g_{\rm amc}|a_0|$ is an effective coupling. In addition, we choose a_0 as a real positive number (we have ignored the phase of a_0). It should be noted that, by supposing the power of the driving field to be about a milliwatt, i.e., $P_d \sim$ mW, we will obtain the effective coupling $g_{\rm eff}$ in the Hz–kHz range, which is an important factor to have for the magnon-CM entanglement. It is clear from Eqs. (10) that the fluctuations of the cavity mode are decoupled from the other modes of the hybrid magnonic system. In this case, the system is reduced effectively into two subsystems in which the magnon mode in the microwave regime is coupled to the CM of the YIG sphere as the external degrees of freedom. Now, we can rewrite the above equations in terms of quadrature fluctuations as follows:

$$\delta\dot{u}(t) = A\delta u(t) + Q. \tag{11}$$

Here $\delta u = (\delta X_m, \delta Y_m, \delta X_c, \delta Y_c)^T$, the quadrature fluctuation operators are defined as $\delta X_o \equiv \frac{\delta o + \delta o^\dagger}{\sqrt{2}}$ and $\delta Y_o \equiv \frac{\delta o - \delta o^\dagger}{\sqrt{2}i}$, and the drift matrix A is given by

$$A = \begin{pmatrix} -\frac{\gamma_m}{2} + \rho\cos\theta & \Delta_m + \rho\sin\theta & 0 & 0 \\ -\Delta_m + \rho\sin\theta & -\frac{\gamma_m}{2} - \rho\cos\theta & 2g_{\rm eff} & 0 \\ 0 & 0 & -\frac{\gamma_c}{2} & \omega_c \\ 2g_{\rm eff} & 0 & -\omega_c & -\frac{\gamma_c}{2} \end{pmatrix}. \tag{12}$$

Also, similarly the noise quadratures are defined as $X_o^{\rm in} \equiv \frac{o^{\rm in} + o^{in\dagger}}{\sqrt{2}}$ and $Y_o^{\rm in} \equiv \frac{o^{\rm in} - o^{in\dagger}}{\sqrt{2}i}$, and the vector $Q = (\sqrt{\gamma_m}X_m^{\rm in}, \sqrt{\gamma_m}Y_m^{\rm in}, \sqrt{\gamma_c}X_c^{\rm in}, \sqrt{\gamma_c}X_c^{\rm in})$ is the noise vector.

It should be mentioned that the hybrid magnomechanical system's stability is controlled by the Routh-Hurwitz criterion [79]. In fact, the system is stable only if all the eigenvalues of the drift matrix have negative real parts. According to this criterion, we have selected the parameters so that the cavity-magnomechanical system with a levitated YIG sphere will be stable. Moreover, because we are applying the linearized quantum Langevin equations and also because the input noises have Gaussian nature, the Gaussian state of the system will be preserved. So, the steady state of the system will be characterized by its 4×4 covariance matrix (CVM):

$$V_{ij} = \frac{\langle u_i(t)u_j(t) + u_j(t)u_i(t)\rangle}{2}. \tag{13}$$

In addition, the steady state of the CVM can be obtained by letting $t \to \infty$ in the above equation and solving the Lyapunov equation:

$$A\,V + V\,A^T = -D, \tag{14}$$

where the diffusion matrix is given by

$$D^T = \mathrm{diag}(\gamma_m n_m, \gamma_m n_m, \gamma_c n_c, \gamma_c n_c), \tag{15}$$

with $n_{m(c)} \equiv (\bar{n}_{m(c)} + 1/2)$. In next section, we demonstrate the magnon-CM entanglement in the cavity-magnomechanical system by applying the logarithmic negativity.

III. MAGNON–CENTER-OF-MASS MOTION ENTANGLEMENT

In this section, to investigate the bipartite entanglement between the magnon and CM modes, we calculate the logarithmic negativity which is defined as [80]

$$E_N = \mathrm{Max}[0, -\ln 2 v_-], \tag{16}$$

where the lowest symplectic eigenvalue of the partial transpose of CVM, v_-, is given by

$$v_- = \tfrac{1}{2}[\Sigma(V)^2 - \sqrt{\Sigma(V)^2 - 4\mathrm{Det}V}]^{1/2}, \tag{17}$$

with $\Sigma(V) \equiv \mathrm{Det}V_m + \mathrm{Det}V_c - 2\mathrm{Det}V_{mc}$. In addition, we have used the following form of the CVM:

$$V = \begin{pmatrix} V_m & V_{mc} \\ V_{mc}^T & V_c \end{pmatrix}, \tag{18}$$

where

$$V_m \equiv \begin{pmatrix} V_{11} & V_{12} \\ V_{21} & V_{22} \end{pmatrix} \quad \text{and} \quad V_c \equiv \begin{pmatrix} V_{33} & V_{34} \\ V_{43} & V_{44} \end{pmatrix} \tag{19}$$

are the 2×2 sub-block matrices associated with the magnon and the CM modes, respectively, and

$$V_{mc} \equiv \begin{pmatrix} V_{13} & V_{14} \\ V_{23} & V_{24} \end{pmatrix} \tag{20}$$

is the sub-block matrix related to their correlation.

In the following, we investigate the MCE in our hybrid magnonic system, in the two situations of the absence and the presence of the magnon squeezing. That is, we investigate the role of squeezing in the nonclassical correlations.

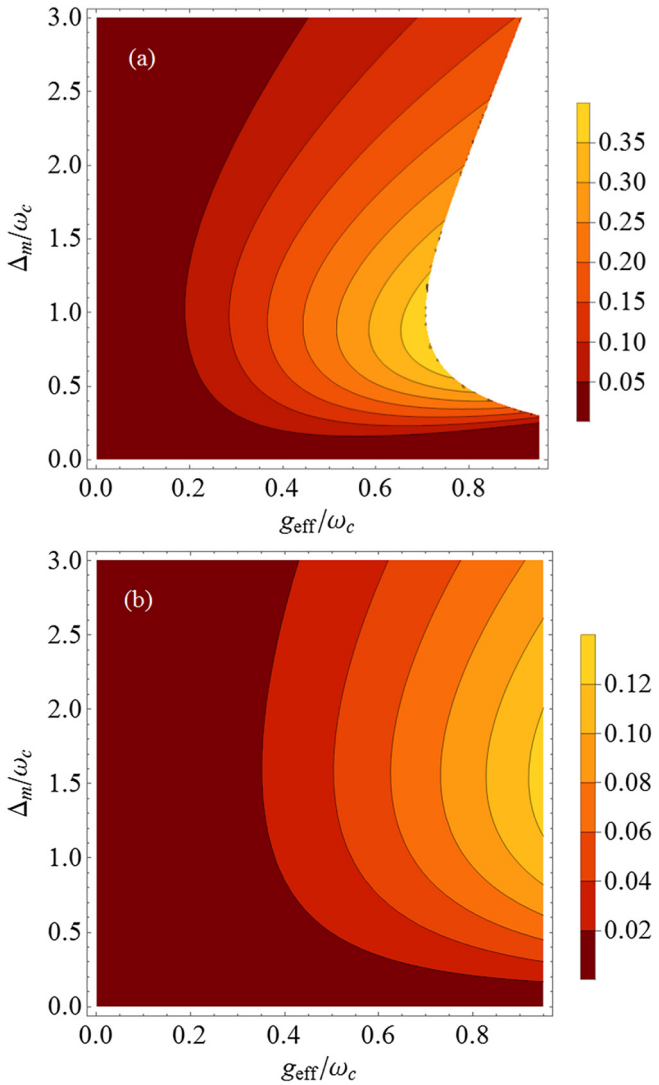

FIG. 2. Magnon-CM entanglement versus the normalized detuning frequency Δ_m/ω_c and the effective coupling $g_{\mathrm{eff}}/\omega_c$ for (a) $\gamma_m/2\pi = 0.1$ MHz and (b) $\gamma_m/2\pi = 0.24$ MHz. The parameters are selected as follows: $\omega_m/2\pi = 30$ GHz, $\gamma_c/2\pi = 10^{-3}$ Hz, $\omega_c/2\pi = 50$ kHz, and $T = 10$ mK [3,15].

In the first setup, we ignore the magnon squeezing, i.e., we assume $\rho = 0$. In this situation, we consider MCE by using the logarithmic negativity, Eq. (16). In Fig. 2, we have plotted E_N versus the normalized detuning frequency Δ/ω_c and the effective coupling strength $g_{\mathrm{eff}}/\omega_c$. Obviously, the MCE has considerable enhancement by increasing the effective coupling strength. Besides, the magnon-CM modes show entanglement in a wide range of detuning frequency, especially around $\Delta_m \simeq \omega_c$. Additionally, considering an ultrapure YIG, the damping rate of the magnon mode, $\gamma_m/2\pi$, can be smaller than the order of MHz. [3,15]. So, by supposing $\gamma_m/2\pi = 0.1$ MHz, we have an MCE of more than 0.35 as shown in Fig. 2(a). However, when we increase the damping rate of the magnon (i.e., $\gamma_m/2\pi = 0.24$ MHz [3]), the bipartite entanglement E_N decreases, as is shown in Fig. 2(b). The other parameters are chosen as $\omega_m/2\pi = 30$ GHz, $\omega_c/2\pi = 50$ kHz, and $\gamma_c/2\pi = 10^{-3}$ Hz. [15].

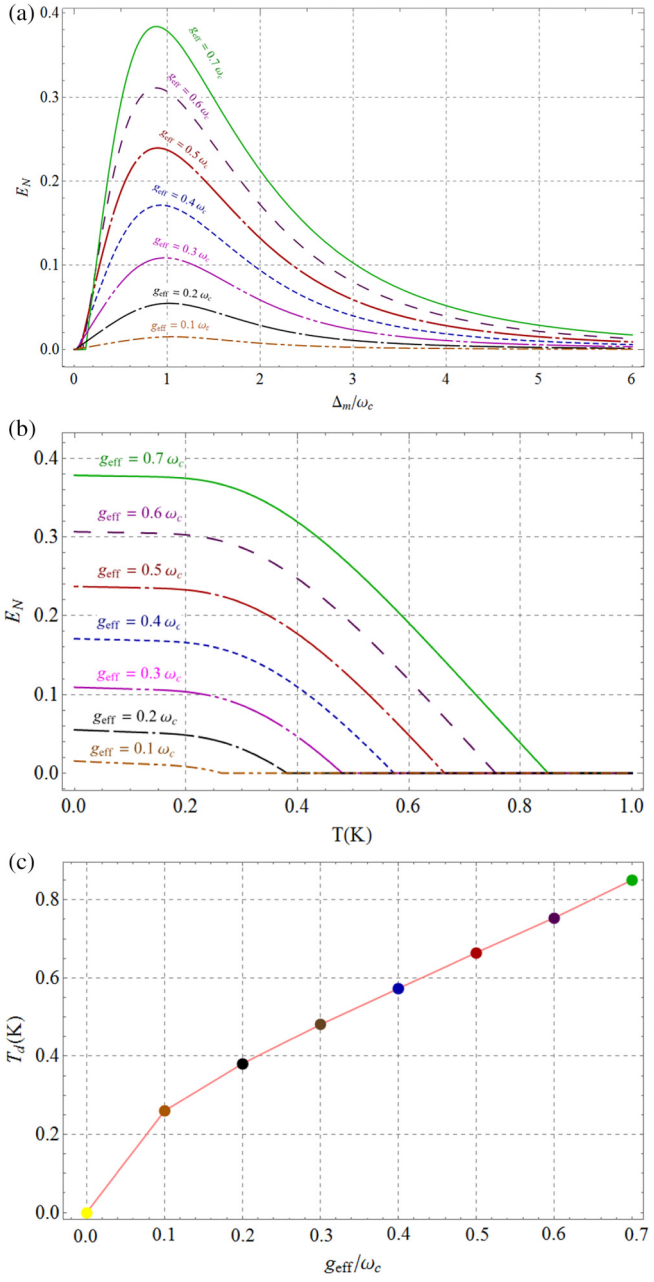

FIG. 3. Magnon-CM entanglement versus (a) the normalized detuning frequency Δ_m/ω_c ($T = 10\,\text{mK}$) and (b) temperature T K ($\Delta_m = \omega_c$) for various effective couplings: $g_{\rm eff} = 0.7\omega_c$ (solid green line), $g_{\rm eff} = 0.6\omega_c$ (dashed purple line), $g_{\rm eff} = 0.5\omega_c$ (dot-dashed red line), $g_{\rm eff} = 0.4\omega_c$ (dotted blue line), $g_{\rm eff} = 0.3\omega_c$ (dot-dot-dashed pink line), $g_{\rm eff} = 0.2\omega_c$ (dash-dash-dotted black line), and $g_{\rm eff} = 0.1\omega_c$ (dash-dash-dot-dotted brown line). (c) The entanglement death's temperature, T_d, versus the effective coupling, $g_{\rm eff}/\omega_c$. Damping rate $\gamma_m/2\pi = 0.1\,\text{MHz}$ and the other parameters are the same as those in Fig. 2(a).

To get more insight, in Fig. 3(a), the MCE has been plotted versus the normalized detuning frequency, Δ/ω_c, for various values of the effective coupling strength: $g_{\rm eff} = 0.7\omega_c$ (solid green line), $g_{\rm eff} = 0.6\omega_c$ (dashed purple line), $g_{\rm eff} = 0.5\omega_c$ (dot-dashed red line), $g_{\rm eff} = 0.4\omega_c$ (dotted blue line), $g_{\rm eff} = 0.3\omega_c$ (dot-dot-dashed pink line), and $g_{\rm eff} = 0.2\omega_c$ (dash-dash-dotted black line), $g_{\rm eff} = 0.1\omega_c$ (dash-dash-dot-dotted brown line). As previously noted, by increasing the effective coupling strength, especially in the vicinity of resonance $\Delta \simeq \omega_c$, we have the maximum values of entanglement. It should be noted that we can increase the effective coupling strength by a strong external driving field. Therefore, the power and frequency of the driving field as two controllable parameters have a significant role in entanglement enhancement.

In addition, in Fig. 3(b) we have plotted the MCE versus the temperature T for various values of the effective coupling strength. As is evident, the temperature increasing will lead to entanglement decrement between the magnon and CM modes. This figure shows that entanglement death occurs at a specific temperature. Thus, we define a death temperature, T_d, as the temperature which induces a transition from the nonzero to the zero MCE. In Fig 3(c), we show the entanglement death's temperature, T_d, in terms of the effective coupling, $g_{\rm eff}/\omega_c$. Interestingly, by increasing the effective coupling, we can preserve the two-mode entanglement at the higher temperature ranges. As is known, when the magnon damping rate is increased, the MCE decreases considerably. So, for preserving this bipartite entanglement, in the following we consider the

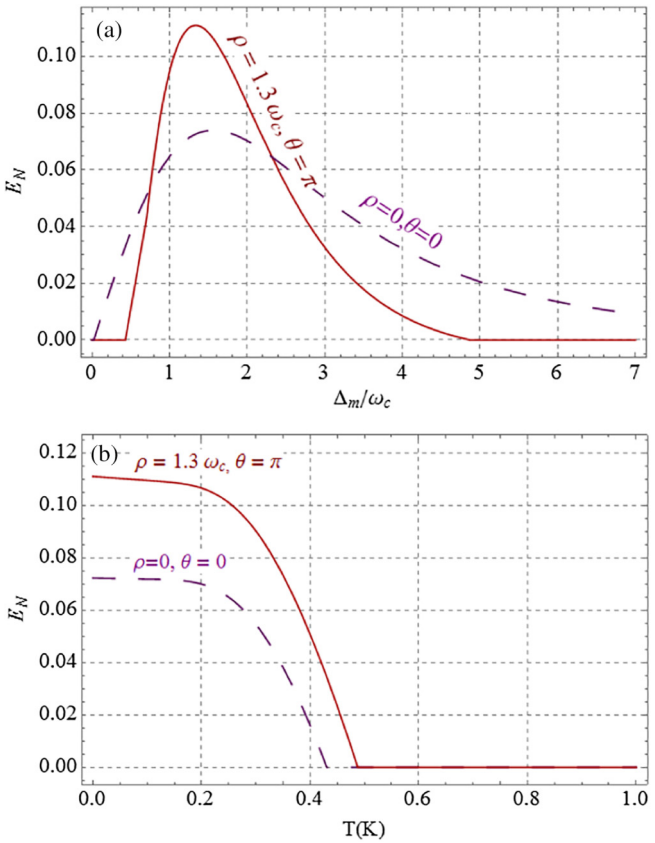

FIG. 4. Magnon-CM entanglement versus (a) the normalized detuning frequency Δ_m/ω_c with $T = 10\,\text{mK}$ and (b) the temperature T with $\Delta_m = 1.3\omega_c$ in the presence and absence of the magnon squeezing, solid red line and dashed purple line, respectively, by $\gamma_m/2\pi = 0.24\,\text{MHz}$ and $g_{\rm eff} = 0.7\omega_c$. The other parameters are the same as those in Fig. 2(b).

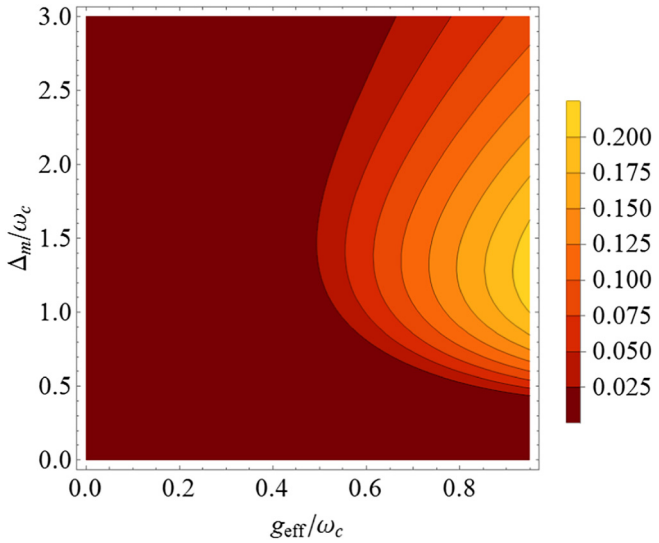

FIG. 5. Magnon-CM entanglement versus the normalized detuning frequency Δ_m/ω_c and the effective coupling $g_{\rm eff}/\omega_c$, in the presence of the magnon squeezing. The parameters are the same as those in Fig. 2(b).

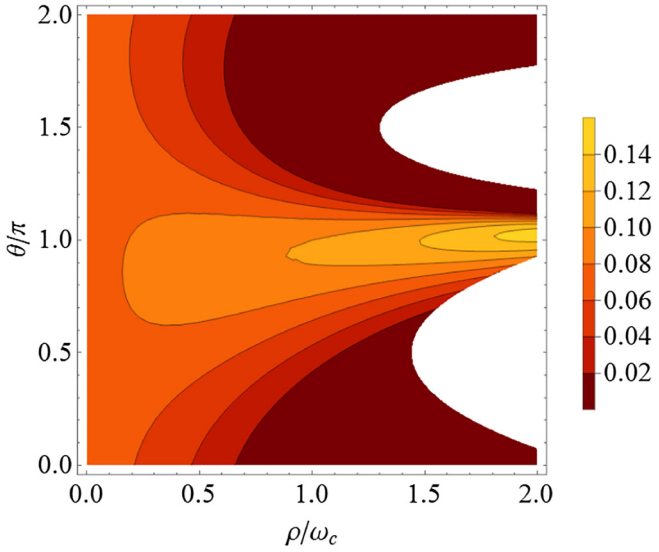

FIG. 6. Magnon-CM entanglement versus the normalized squeezing parameters ρ/ω_c and the phase θ/π with $g_{\rm eff} = 0.7\omega_c$ and $\Delta_m = 1.3\omega_c$. The parameters are the same as those in Fig. 2(b).

magnon squeezing [74,75,81], i.e., $\rho \neq 0$, and we study the influence of this nonclassical effect on the MCE.

In the second setup, we concentrate on the role of magnon squeezing, as a nonclassical effect, on the enhancement and the manipulation of the MCE. To obtain more insights about the effects of magnon squeezing, in Fig. 4, we have plotted the MCE versus the normalized detuning frequency, Δ_m/ω_c, and the temperature, T, in the presence (red line) and absence (blue line) of the magnon squeezing. As it is seen, by enhancing the damping rate of the magnon, we can see the MCE up to the temperature of 250 mK. Furthermore, in Fig. 5 the MCE has been plotted versus the normalized detuning frequency Δ_m/ω_c and the effective coupling $g_{\rm eff}/\omega$. A comparison between Figs. 5 and 2(b) clearly shows that the MCE increases due to magnon squeezing, while magnon damping rate is enhanced in comparison with Fig. 2(a). In Fig. 6 the MCE has been plotted versus the squeezing parameter ρ and the phase θ. It should be noted that the MCE increases by enhancing the squeezing parameter. In addition, the maximum of the entanglement happens around $\theta = \pi$. Interestingly, this nonclassical effect allows us to manipulate entanglement through two squeezing parameters. As is mentioned before, the hybrid magnomechanical system's stability is determined by the Routh-Hurwitz criterion. Therefore, it is worth noting that the blank, uncalculated parameters in Figs. 2(a) and 6 demonstrate the system is unstable for these parameters.

Remark. One of the most convenient measures for the squeezing is expressed in the dB unit, given by $-10\,\mathrm{Log}_{10}[\langle(\delta X_m)^2\rangle/\langle(\delta X_m)^2\rangle_{\rm vac}]$, where $\langle(\delta X_m)^2\rangle_{\rm vac} = 0.5$ denotes the vacuum fluctuations [26,82]. The variance $\langle(\delta X_m)^2\rangle$ can be determined in terms of the CVM elements, so that for the magnon mode we have $\langle(\delta X_m)^2\rangle = V_{11}$. It is worth noting that, for the parameters that we used, the level of magnon squeezing is approximately 1 dB.

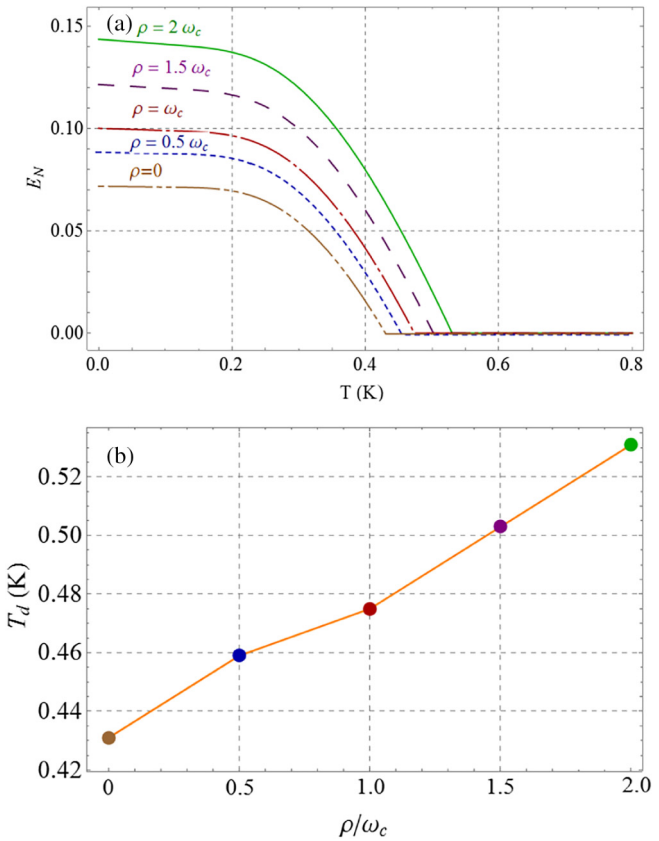

FIG. 7. (a) Magnon-CM entanglement versus temperature T (K) for various magnon squeezing parameters: $\rho = 2\omega_c$ (solid green line), $\rho = 1.5\omega_c$ (dashed purple line), $\rho = \omega_c$ (dot-dashed red line), $\rho = 0.5\omega_c$ (dotted blue line), and $\rho = 0$ (dot-dot-dashed brown line). (b) The entanglement death's temperature T_d versus the normalized magnon squeezing parameter ρ/ω_c. The damping rate $\gamma_m/2\pi = 0.24$ MHz, the effecting coupling $g_{\rm eff} = 0.7\omega_c$, the detuning frequency $\Delta_m = 1.3\omega_c$, and the other parameters are the same as those in Fig 2(b).

In addition, in Fig. 7(a) we have plotted the MCE versus the temperature T for different values of magnon squeezing parameters: $\rho = 2\omega_c$ (solid green line), $\rho = 1.5\omega_c$ (dashed purple line), $\rho = \omega_c$ (dot-dashed red line), $\rho = 0.5\omega_c$ (dotted blue line), and $\rho = 0$ (dot-dot-dashed brown line). As mentioned before, the MCE decreases by increasing temperatures, but if we look at the entanglement death's temperature T_d versus the normalized magnon squeezing parameters, as illustrated in Fig. 7(b), by enhancing the magnon squeezing, we can preserve the MCE at higher temperatures. As an important result, we find that by changing the magnon squeezing, we can control this bipartite entanglement. In order to understand the physical reason of this behavior, we must note that increasing the magnon squeezing parameter ρ causes the nonlinearity of the system to be enhanced and finally causes the entanglement to increase. Moreover, the MCE is sensitive to temperature and the nonlinearity induced by magnon squeezing helps to preserve the entanglement at higher temperatures.

Finally, let us discuss how to measure the bipartite entanglement. In order to measure E_N at the steady state, one needs to measure the CVM [23,83]. Also, by sending a weak microwave probe field and homodyning the cavity output of the probe field, we can read out the magnon state. This approach requires that the dissipation rate of the magnon mode be smaller than the dissipation rate of the cavity mode, such that when the drive field is switched off and all cavity photons are decayed, the magnon state remains almost unchanged [20]. However, a better approach would be to detect entanglement indirectly. It means that using indirect measurement, the magnon state and the mechanical state read out separately, utilizing auxiliary cavities with beam-splitter-like interactions with those two modes [83,84].

IV. CONCLUSION AND OUTLOOK

We have proposed a scheme for formation of entanglement in a cavity magnomechanical system, including a levitated YIG sphere micromagnet. In fact, by supposing that the YIG sphere is trapped in the node of the cavity magnetic field, the effective coupling that is independent of mass and size of the YIG sphere arises between magnon and CM and is increased by increasing the driving field. We find that the entanglement death's temperature increases by enhancing the effective coupling.

However, by increasing the magnon damping rate, this entanglement considerably decreases. Therefore, for enhancing the MCE, we assume the magnon squeezing and we demonstrate that this nonclassical effect has a significant role in the manipulation and increment of MCE. In other words, magnon squeezing gives us the opportunity to preserve this entanglement at elevated temperatures even if the magnon damping rate increases. Interestingly, this entanglement between the external and internal degrees of freedom finds potential application in the study of macroscopic quantum phenomena. Since the CM degrees freedom are external degrees of freedom, their manipulation is possible. Thus, with these external degrees of freedom we can manipulate the magnon degrees of freedom. Therefore, the entanglement between magnons and CM provides this opportunity to manipulate the magnon subsystem.

[1] Y. Tabuchi, S. Ishino, T. Ishikawa, R. Yamazaki, K. Usami, and Y. Nakamura, Hybridizing ferromagnetic magnons and microwave photons in the quantum limit, Phys. Rev. Lett. **113**, 083603 (2014).

[2] H. Huebl, C. W. Zollitsch, J. Lotze, F. Hocke, M. Greifenstein, A. Marx, R. Gross, and S. T. Goennenwein, High cooperativity in coupled microwave resonator ferrimagnetic insulator hybrids, Phys. Rev. Lett. **111**, 127003 (2013).

[3] X. Zhang, C.-L. Zou, L. Jiang, and H. X. Tang, Strongly coupled magnons and cavity microwave photons, Phys. Rev. Lett. **113**, 156401 (2014).

[4] H. Maier-Flaig, S. Klingler, C. Dubs, O. Surzhenko, R. Gross, M. Weiler, H. Huebl, and S. T. B. Goennenwein, Temperature-dependent magnetic damping of yttrium iron garnet spheres, Phys. Rev. B **95**, 214423 (2017).

[5] L. Bai, M. Harder, Y. P. Chen, X. Fan, J. Q. Xiao, and C. M. Hu, Spin pumping in electrodynamically coupled magnon-photon systems, Phys. Rev. Lett. **114**, 227201 (2015).

[6] N. J. Lambert, J. A. Haigh, S. Langenfeld, A. C. Doherty, and A. J. Ferguson, Cavity-mediated coherent coupling of magnetic moments, Phys. Rev. A **93**, 021803(R) (2016).

[7] D. Lachance-Quirion, Y. Tabuchi, S. Ishino, A. Noguchi, T. Ishikawa, R. Yamazaki, and Y. Nakamura, Resolving quanta of collective spin excitations in a millimeter-sized ferromagnet, Sci. Adv. **3**, e1603150 (2017).

[8] R. Hisatomi, A. Osada, Y. Tabuchi, T. Ishikawa, A. Noguchi, R. Yamazaki, K. Usami, and Y. Nakamura, Bidirectional conversion between microwave and light via ferromagnetic magnons, Phys. Rev. B **93**, 174427 (2016).

[9] T. Liu, X. Zhang, H. X. Tang, and M. E. Flatté, Optomagnonics in magnetic solids, Phys. Rev. B **94**, 060405(R) (2016).

[10] S. Viola Kusminskiy, H. X. Tang, and F. Marquardt, Coupled spin-light dynamics in cavity optomagnonics, Phys. Rev. A **94**, 033821 (2016).

[11] X. Zhang, N. Zhu, C.-L. Zou, and H. X. Tang, Optomagnonic whispering gallery microresonators, Phys. Rev. Lett. **117**, 123605 (2016).

[12] D. Lachance-Quirion, Y. Tabuchi, A. Gloppe, K. Usami, and Y. Nakamura, Hybrid quantum systems based on magnonics, Appl. Phys. Express **12**, 070101 (2019).

[13] C. Gonzalez-Ballestero, D. Hümmer, J. Gieseler, and O. Romero-Isart, Theory of quantum acoustomagnonics and acoustomechanics with a micromagnet, Phys. Rev. B **101**, 125404 (2020).

[14] C. Gonzalez-Ballestero, J. Gieseler, and O. Romero-Isart, Quantum acoustomechanics with a micromagnet, Phys. Rev. Lett. **124**, 093602 (2020).

[15] A. Kani, B. Sarma, and J. Twamley, Intensive Cavity-magnomechanical cooling of a Levitated macromagnet, Phys. Rev. Lett. **128**, 013602 (2022).

[16] M.-S. Ding, L. Zheng, and C. Li, Ground-state cooling of a magnomechanical resonator induced by magnetic damping, J. Opt. Soc. Am. B **37**, 627 (2020).

[17] Z.-X. Yang, L. Wang, Y.-M. Liu, D.-Y. Wang, C.-H. Bai, S. Zhang, and H.-F. Wang, Ground state cooling of magnomechanical resonator in $\mathcal{PT}$-symmetric cavity magnomechanical system at room temperature, Front. Phys. **15**, 52504 (2020).

[18] A. V. Chumak, V. I. Vasyuchka, A. A. Serga, and B. Hillebrands, Magnon spintronics, Nat. Phys. **11**, 453 (2015).

[19] L. Bai, M. Harder, P. Hyde, Z. Zhang, C.-M. Hu, Y. P. Chen, and J. Q. Xiao, Cavity mediated manipulation of distant spin currents using a cavity-magnon-polariton, Phys. Rev. Lett. **118**, 217201 (2017).

[20] J. Li, S.-Y. Zhu, and G. S. Agarwal, Magnon-photon-phonon entanglement in cavity magnomechanics, Phys. Rev. Lett. **121**, 203601 (2018).

[21] J. Li and S.-Y. Zhu, Entangling two magnon modes via magnetostrictive interaction, New J. Phys. **21**, 085001 (2019).

[22] M. Yu, H. Shen, and J. Li, Magnetostrictively induced stationary entanglement between two microwave fields, Phys. Rev. Lett. **124**, 213604 (2020).

[23] J. Li and S. Gröblacher, Entangling the vibrational modes of two massive ferromagnetic spheres using cavity magnomechanics, Quantum Sci. Technol. **6**, 024005 (2021).

[24] Y.-T. Chen, L. Du, Y. Zhang, and J.-H. Wu, Perfect transfer of enhanced entanglement and asymmetric steering in a cavity-magnomechanical system, Phys. Rev. A **103**, 053712 (2021).

[25] M.-S. Ding, X.-X. Xin, S.-Y. Qin, and C. Li, Enhanced entanglement and steering in $\mathcal{PT}$-symmetric cavity magnomechanics, Opt. Commun. **490**, 126903 (2021).

[26] J. Li, S.-Y. Zhu, and G. S. Agarwal, Squeezed states of magnons and phonons in cavity magnomechanics, Phys. Rev. A **99**, 021801(R) (2019).

[27] Y. S. Ihn, S.-Y. Lee, D. Kim, S. H. Yim, and Z. Kim, Coherent multimode conversion from microwave to optical wave via a magnon-cavity hybrid system, Phys. Rev. B **102**, 064418 (2020).

[28] C.-Z. Chai, Z. Shen, Y.-L. Zhang, H.-Q. Zhao, G.-C. Guo, C.-L. Zou, and C.-H. Dong, Single-sideband microwave-to-optical conversion in high-Q ferrimagnetic microspheres, Photonics Res. **10**, 820 (2022).

[29] Y.-P. Wang, J. W. Rao, Y. Yang, P.-C. Xu, Y. S. Gui, B. M. Yao, J. Q. You, and C.-M. Hu, Nonreciprocity and unidirectional invisibility in cavity magnonics, Phys. Rev. Lett. **123**, 127202 (2019).

[30] Y. T. Zhao, J. W. Rao, Y. S. Gui, Y. P. Wang, and C.-M. Hu, Broadband nonreciprocity realized by locally controlling the magnon's radiation, Phys. Rev. Appl. **14**, 014035 (2020).

[31] T. Trickle, Z. Zhang, and K. M. Zurek, Detecting light dark matter with magnons, Phys. Rev. Lett. **124**, 201801 (2020).

[32] S. P. Wolski, D. Lachance-Quirion, Y. Tabuchi, S. Kono, A. Noguchi, K. Usami, and Y. Nakamura, Dissipation-based quantum sensing of magnons with a superconducting qubit, Phys. Rev. Lett. **125**, 117701 (2020).

[33] M. S. Ebrahimi, A. Motazedifard, and M. B. Harouni, Single-quadrature quantum magnetometry in cavity electromagnonics, Phys. Rev. A **103**, 062605 (2021).

[34] D. Lachance-Quirion, S. Piotr Wolski, Y. Tabuchi, S. Kono, K. Usami, and Y. Nakamura, Entanglement-based single-shot detection of a single magnon with a superconducting qubit, Science **367**, 425 (2020).

[35] X. Zhang, C.-L. Zou, N. Zhu, F. Marquardt, L. Jiang, and H. X. Tang, Magnon dark modes and gradient memory, Nat. Commun. **6**, 8914 (2015).

[36] R.-C. Shen, Y.-P. Wang, J. Li, S.-Y. Zhu, G. S. Agarwal, and J. Q. You, Long-time memory and ternary logic gate using a multistable cavity magnonic system, Phys. Rev. Lett. **127**, 183202 (2021).

[37] S.-N. Huai, Y.-L. Liu, J. Zhang, L. Yang, and Y.-X. Liu, Enhanced sideband responses in a $\mathcal{PT}$-symmetric-like cavity magnomechanical system, Phys. Rev. A **99**, 043803 (2019).

[38] K. Ullah, M. T. Naseem, and O. E. MüstecaplioğluÄ±oglu, Tunable multiwindow magnomechanically induced transparency, Fano resonances, and slow-to-fast light conversion, Phys. Rev. A **102**, 033721 (2020).

[39] B. Wang, X. Jia, X.-H. Lu, and H. Xiong, $\mathcal{PT}$-symmetric magnon laser in cavity optomagnonics, Phys. Rev. A **105**, 053705 (2022).

[40] Z.-X. Liu and H. Xiong, Magnon laser based on Brillouin light scattering, Opt. Lett. **45**, 5452 (2020).

[41] C. A. Potts, V. A. S. V. Bittencourt, S. V. Kusminskiy, and J. P. Davis, Magnon-phonon quantum correlation thermometry, Phys. Rev. Appl. **13**, 064001 (2020).

[42] D. Zhang, X.-Q. Luo, Y.-P. Wang, T.-F. Li, and J. Q. You, Observation of the exceptional point in cavity magnon-polaritons, Nat. Commun. **8**, 1368 (2017).

[43] B. Wang, Z.-X. Liu, C. Kong, H. Xiong, and Y. Wu, Magnon induced transparency and amplification in $\mathcal{PT}$-symmetric cavity-magnon system, Opt. Express **26**, 20248 (2018).

[44] G.-Q. Zhang and J. Q. You, Higher-order exceptional point in a cavity magnonics system, Phys. Rev. B **99**, 054404 (2019).

[45] X. Zhang, K. Ding, X. Zhou, J. Xu, and D. Jin, Experimental observation of an exceptional surface in synthetic dimensions with magnon polaritons, Phys. Rev. Lett. **123**, 237202 (2019).

[46] Y. Cao and P. Yan, Exceptional magnetic sensitivity of $\mathcal{PT}$-symmetric cavity magnon polaritons, Phys. Rev. B **99**, 214415 (2019).

[47] A. T. M. Anishur Rahman, Large spatial Schrödinger cat state using a levitated ferrimagnetic nanoparticle, New J. Phys. **21**, 113011 (2019).

[48] C. C. Rusconi, V. Pöchhacker, K. Kustura, J. I. Cirac, and O. Romero-Isart, Quantum spin stabilized magnetic levitation, Phys. Rev. Lett. **119**, 167202 (2017).

[49] J. Gieseler, A. Kabcenell, E. Rosenfeld, J. D. Schaefer, A. Safira, M. J. A. Schuetz, C. Gonzalez-Ballestero, C. C. Rusconi, O. Romero Isart, and M. D. Lukin, Single-spin magnetomechanics with levitated micromagnets, Phys. Rev. Lett. **124**, 163604 (2020).

[50] T. Seberson, P. Ju, J. Ahn, J. Bang, T. Li, and F. Robicheaux, Simulation of sympathetic cooling an optically levitated magnetic nanoparticle via coupling to a cold atomic gas, J. Opt. Soc. Am. B **37**, 3714 (2020).

[51] A. Vinante, G. Wijts, O. Usenko, L. Schinkelshoek, and T. H. Oosterkamp, Magnetic resonance force microscopy of paramagnetic electron spins at millikelvin temperatures, Nat. Commun. **2**, 572 (2011).

[52] R. Fischer, D. P. McNally, C. Reetz, G. G. T. Assumpčão, T. Knief, Y. Lin, and C. A. Regal, Spin detection with a micromechanical trampoline: Towards magnetic resonance microscopy

harnessing cavity optomechanics, New J. Phys. **21**, 043049 (2019).
[53] N. K. Raut, J. Miller, J. Pate, R. Chiao, and J. E. Sharping, Meissner levitation of a millimeter-size neodymium magnet within a superconducting radio frequency cavity, IEEE Trans. Appl. Supercond. **31**, 1500204 (2021).
[54] C. Timberlake, G. Gasbarri, A. Vinante, A. Setter, and H. Ulbricht, Acceleration sensing with magnetically levitated oscillators above a superconductor, Appl. Phys. Lett. **115**, 224101 (2019).
[55] P. Huillery, T. Delord, L. Nicolas, M. Van Den Bossche, M. Perdriat, and G. Hetet, Spin mechanics with levitating ferromagnetic particles, Phys. Rev. B **101**, 134415 (2020).
[56] M. Fuwa, R. Sakagami, and T. Tamegai, Ferromagnetic levitation and harmonic trapping of a milligram-scale yttrium iron garnet sphere, Phys. Rev. A **108**, 063511 (2023).
[57] U. Delić, M. Reisenbauer, K. Dare, D. Grass, V. Vuletić, N. Kiesel, and M. Aspelmeyer, Cooling of a levitated nanoparticle to the motional quantum ground state, Science **367**, 892 (2020).
[58] G. Ranjit, M. Cunningham, K. Casey, and A. A. Geraci, Zeptonewton force sensing with nanospheres in an optical lattice, Phys. Rev. A **93**, 053801 (2016).
[59] D. C. Moore and A. A. Geraci, Searching for new physics using optically levitated sensors, Quantum Sci. Technol. **6**, 014008 (2021).
[60] C. Marletto and V. Vedral, Gravitationally induced entanglement between two massive particles is sufficient evidence of quantum effects in gravity, Phys. Rev. Lett. **119**, 240402 (2017).
[61] J. Gieseler, R. Quidant, C. Dellago, and L. Novotny, Dynamic relaxation of a levitated nanoparticle from a non-equilibrium steady state, Nat. Nanotechnol. **9**, 358 (2014).
[62] C. Gonzalez-Ballestero, M. Aspelmeyer, L. Novotny, R. Quidant, and O. Romero-Isart, Levitodynamics: Levitation and control of microscopic objects in vacuum, Science **374**, eabg3027 (2021).
[63] W. J. Munro, K. Nemoto, G. J. Milburn, and S. J. Braunstein (2002), Weak-force detection with superposed coherent states, Phys. Rev. A **66**, 023819 (2002).
[64] P. T. Cochrane, G. J. Milburn, and W. J. Munro, Macroscopically distinct quantum-superposition states as a bosonic code for amplitude damping, Phys. Rev. A **59**, 2631 (1999).
[65] S. Alam, M. Sh. Hossain, S. R. Srinivasa, and A. Aziz, Cryogenic memory technologies, Nat. Electron. **6**, 185 (2023).
[66] S. J. van Enk, and O. Hirota, Entangled coherent states: Teleportation and decoherence, Phys. Rev. A **64**, 022313 (2001).
[67] X. Wang, Quantum teleportation of entangled coherent states, Phys. Rev. A **64**, 022302 (2001).
[68] G. Tóth, C. Knapp, O. Gühne, and H. J. Briegel, Spin squeezing and entanglement, Phys. Rev. A **79**, 042334 (2009).
[69] A. Abramovici, W. E. Althouse, R. W. P. Drever, Y. Gürsel, S. Kawamura, F. J. Raab, D. Shoemaker, L. Sievers, R. E. Spero, K. S. Thorne, R. E. Vogt, R. Weiss, S. E. Whitcomb, and M. E. Zucker, LIGO: The laser interferometer gravitational-wave observatory, Science **256**, 325 (1992).
[70] W. Zhao, S.-D. Zhang, A. Miranowicz, and H. Jing, Weak-force sensing with squeezed optomechanics, Sci. China: Phys., Mech. Astron. **63**, 224211 (2020).
[71] A. Furusawa, J. L. Sørensen, S. L. Braunstein, C. A. Fuchs, H. J. Kimble, and E. S. Polzik, Unconditional quantum teleportation, Science **282**, 706 (1998).
[72] M. S. Ding, L. Zheng, Y. Shi, and Y. J. Liu, Magnon squeezing enhanced entanglement in a cavity magnomechanical system, J. Opt. Soc. Am. B **39**, 2665 (2022).
[73] A. Sohail, R. Ahmed, J. X. Peng, A. Shahzad, S. K. Singh, Enhanced entanglement via magnon squeezing in a two-cavity magnomechanical system, J. Opt. Soc. Am. B **40**, 1359 (2023).
[74] A. Kamra and W. Belzig, Super-Poissonian shot noise of squeezed-magnon mediated spin transport, Phys. Rev. Lett. **116**, 146601 (2016).
[75] Q. Guo, J. Cheng, H. Tan, and J. Li, Magnon squeezing by two-tone driving of a qubit in cavity-magnon-qubit systems, Phys. Rev. A **108**, 063703 (2023).
[76] D. Zhang, X.-M. Wang, T.-F. Li, X.-Q. Luo, W. Wu, F. Nori, and J. You, Cavity quantum electrodynamics with ferromagnetic magnons in a small yttrium-iron-garnet sphere, npj Quantum Inf. **1**, 15014 (2015).
[77] Y. Tabuchi, S. Ishino, A. Noguchi, T. Ishikawa, R. Yamazaki, K. Usami, and Y. Nakamura, Quantum magnonics: The magnon meets the superconducting qubit, C. R. Phys. **17**, 729 (2016).
[78] M. Aspelmeyer, T. J. Kippenberg, and F. Marquardt, Cavity optomechanics, Rev. Mod. Phys. **86**, 1391 (2014).
[79] H. G. Bergman, R. Bellman, and R. E. Kalaba, *Selected Papers on Mathematical Trends in Control Theory* (Dover, New York, 1964).
[80] G. Adesso, A. Serafini, and F. Illuminati, Extremal entanglement and mixedness in continuous variable systems, Phys. Rev. A **70**, 022318 (2004).
[81] T. X. Lu, X. Xiao, L. S. Chen, Q. Zhang, and H. Jing, Magnon-squeezing-enhanced slow light and second-order sideband in cavity magnomechanics, Phys. Rev. A **107**, 063714 (2023).
[82] Z. B. Yang, H. Jin, J. W. Jin, J. Y. Liu, H. Y. Liu, and R. Can Yang, Bistability of squeezing and entanglement in cavity magnonics, Phys. Rev. Res. **3**, 023126 (2021).
[83] Z. Zhang, M. O. Scully, and G. S. Agarwal, Quantum entanglement between two magnon modes via Kerr nonlinearity driven far from equilibrium, Phys. Rev. Res. **1**, 023021 (2019).
[84] D. Vitali, S. Gigan, A. Ferreira, H. R. Bohm, P. Tombesi, A. Guerreiro, V. Vedral, A. Zeilinger, and M. Aspelmeyer, Optomechanical entanglement between a movable mirror and a cavity field, Phys. Rev. Lett. **98**, 030405 (2007).